

RSC Advances



This is an *Accepted Manuscript*, which has been through the Royal Society of Chemistry peer review process and has been accepted for publication.

Accepted Manuscripts are published online shortly after acceptance, before technical editing, formatting and proof reading. Using this free service, authors can make their results available to the community, in citable form, before we publish the edited article. This *Accepted Manuscript* will be replaced by the edited, formatted and paginated article as soon as this is available.

You can find more information about *Accepted Manuscripts* in the [Information for Authors](#).

Please note that technical editing may introduce minor changes to the text and/or graphics, which may alter content. The journal's standard [Terms & Conditions](#) and the [Ethical guidelines](#) still apply. In no event shall the Royal Society of Chemistry be held responsible for any errors or omissions in this *Accepted Manuscript* or any consequences arising from the use of any information it contains.

ARTICLE

One-Step Fabrication of RGO/HNBR Composites via Selective Hydrogenation of NBR with Graphene-based Catalyst

Cite this: DOI:
10.1039/x0xx00000x

www.rsc.org/

Peng Cao^a, Changyue Huang^a, Liqun Zhang^{a,b}, Dongmei Yue^{a,b*}

The concept of hydrogenation of NBR using graphene-based catalyst is applied to prepare RGO/HNBR composites. The catalyst is synthesized by reduction of the mixture of a rhodium salt and dispersed graphite oxide sheets. Compared with HNBR, the obtained composite exhibits enhanced mechanical and electrical properties.

Hydrogenation of acrylonitrile butadiene rubber (NBR) is a representative example to produce hydrogenated acrylonitrile butadiene rubber (HNBR), a polymer that shows more resistance than NBR toward oxidative and ozonolytic aging while maintaining its resistance to oils in rigorous chemical environments as well as remarkable improvements in mechanical properties.¹

Generally, the NBR hydrogenation is carried out over heterogeneous^{2,3} or homogeneous⁴⁻⁶ catalysts based on group VIII metal, such as Pd, Ru, and Rh. For heterogeneous hydrogenation, the characteristics of polymer hydrogenation are quite different from that of small molecules. In polymer hydrogenation, the unsaturated polymer coils need to transport from the bulk liquid phase to the external surface of the support, and then diffuse into the pores to access the active sites on the pore walls.⁷ Because of the large dimension of polymer chain and the high viscosity of the solution, the mass transfer of polymer coils in the solution and the pores of the supports proved extremely challenging.^{8,9} Even though the external diffusion of polymer coils could be enhanced by increasing the agitation rate, the enhancement of pore diffusion of polymer coils is still a difficult issue. Moreover, the adsorption and hydrogenation of polymer chain on active sites are restrained from the steric-hindrance of a large size of polymer coils.

In order to improve the pore diffusion of polymer coils, several methods were proposed, e.g. the supercritical CO₂ technology^{10,11} and optimal structure design of the supports.¹² Supports with high specific surface area and abundant micro- or meso- pores lead to better dispersion of active metal, but most of the active metal particles deposit on the surface of internal pores, resulting in the difficult access of polymer coils to the active sites. On the other hand, the non-porous supports, such as CaCO₃ and BaSO₄, possess active sites on

the external surface and could avoid pore diffusion, but the surface area is limited and the dispersion of active metal on the carrier is poor.⁷ Therefore, the goal of our study is to explore a new support for polymer hydrogenation, which could not only eliminate inner pore diffusion of polymer coils, but also have a high external surface area at the same time.

Graphene, a unique 2D layer of sp²-hybridized carbon, has received much attention both in theoretical studies and applications owing to its extraordinary properties.¹³⁻²⁰ The properties of graphene such as high thermal, chemical, and mechanical stability as well as high surface area (2600 m² g⁻¹, theoretical value) provide an excellent catalyst support for metallic nanoparticles in heterogeneous catalysis.^{17,21-23} Due to its 2D structures, graphene has a little micro-porosity, and a very large external surface area. These specific properties of graphene may shed interesting light on the catalyst exploitation of diene polymer hydrogenation, such as NBR, which has never been reported in the literature. Also, the supported catalysts in hydrogenation of macromolecular polymer usually are difficult to separated from the mixing glue solution due to its high viscosity. However, the remained graphene in the glue solution could be used to prepare graphene-based HNBR composites. In this study, we report for the first time one-step method to prepare RGO/HNBR composites by hydrogenation of NBR with graphene supported Rh catalyst. In this method, graphene acts as a catalyst support as well as filler for enhancing the electronic, and mechanical properties of polymer matrices.

Figure 1 displays the XRD patterns of the graphite powder, prepared GO, and catalyst Rh/RGO. The graphite powder shows the typical sharp diffraction peak at 2θ= 26.7°, while the GO sample shows no diffraction peaks from the parental graphite material and a sharp and strong diffraction peak at 2θ= 10.9°, indicating the distance between the carbon sheets has increased resulting from the insertion of hydroxyl and epoxy groups between the graphite sheets as a result of the oxidation process of graphite.^{21,24,25} Following reduction of the GO, the yellow golden colour of the GO solution changes to black with disappearance of the peak at 2θ=10.9°, suggesting reduction of the GO sheets. The very small sharp peak around 2θ= 26.7° in Rh/RGO was detected, attributing

to the formation of “re-graphitized” carbon regions due to the van der Waals attractive interactions.²¹ Significantly sharp diffraction peaks of Rh were detected for Rh/RGO at 41.07°, 47.78°, 69.88° and 84.40°, which corresponded to the (111), (200), (220) and (311) planes of Rh, respectively. For the FTIR spectra of GO and RGO/Rh (Figure S1), GO shows significant bands around 1060 cm⁻¹ (C-O), 1220 cm⁻¹ (phenolic), 1370 cm⁻¹ (O-H bending in tertiary alcohol), 1620 cm⁻¹ HOH bending in water) and 1720 cm⁻¹ (C=O).²⁶ After reduction, these signals decrease dramatically and are barely detectable. These results indicated that GO was reduced effectively and the highly dispersed Rh NPs formed on the surface of RGO.

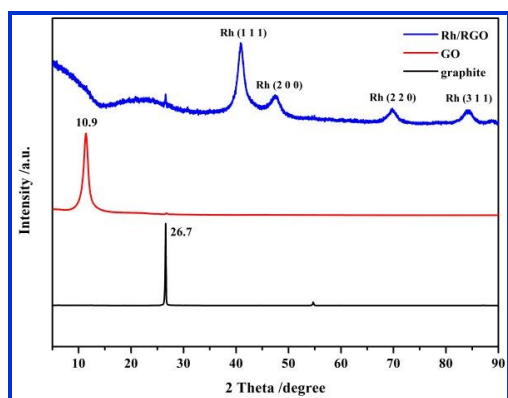


Figure 1 XRD patterns of graphite, GO, and Rh/RGO samples.

Figure 2 shows representative TEM image of the GO and Rh/RGO. It is clear that the presence of uniform well-dispersed Rh nanoparticles on RGO sheets over several microns. The morphology of the GO and Rh/RGO consists of platelets and extended sheets of lateral dimensions with layered structures. Meanwhile, the Raman spectra of the graphite, GO, and RGO/Rh present in Figure S2. Furthermore, the AFM image of GO displays irregular sheets with an average thickness of ~1.00 nm (Figure S3). Considering the thickness of single-layer graphene was about 0.34, it can be concluded that the enhanced sheet thickness observed from GO (~1.00 nm) was possibly ascribed to the multiple layers bridged with large number of oxygen containing groups. However, the thickness of Rh/RGO increases to 2~4 nm, indicating the Rh NPs are well-dispersed on the surface of RGO.

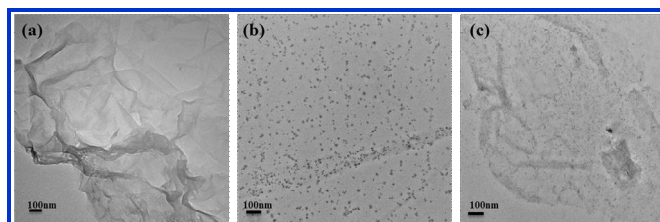


Figure 2 TEM images of (a) GO and (b, c) Rh/RGO.

XPS provide direct evidence for the elemental composition of GO and Rh/RGO, as present in Figure 3. The C/O

atomic ratio (70%/30%) of GO confirms successful oxidation of graphite (Table S2). The C 1s XPS spectrum of GO and Rh/RGO is split into three peaks which can be attributed to carbon atoms with different functional groups, including the C=C (~284.6 eV), C-O (~286.7 eV), C=O (~288.2 eV) and O-C=O (289.5 eV) bonds, respectively.^{17, 21} After reduction, the oxygen containing groups reduced significantly, an efficient deoxidization. The C/O atomic ratio (82%/18%) of graphene confirms that GO has been successfully reduced. However, some oxygen still remains in Rh/RGO and the partial reduction of GO in the presence of the Rh³⁺ could be explained by a competition between the reduction of the Rh³⁺ and GO.

The XPS spectra of the Rh 3d in Rh/RGO show that most of the Rh NPs are present as Rh⁰ in the NaBH₄ system, in accordance with the observed binding energies of 307.3 eV (Rh⁰ 3d_{5/2}) and 312.2 eV (Rh⁰ 3d_{3/2}).²⁷ However, for the N₂H₄·H₂O system, near 98% of Rh NPs are present as Rh³⁺ (Table S2).

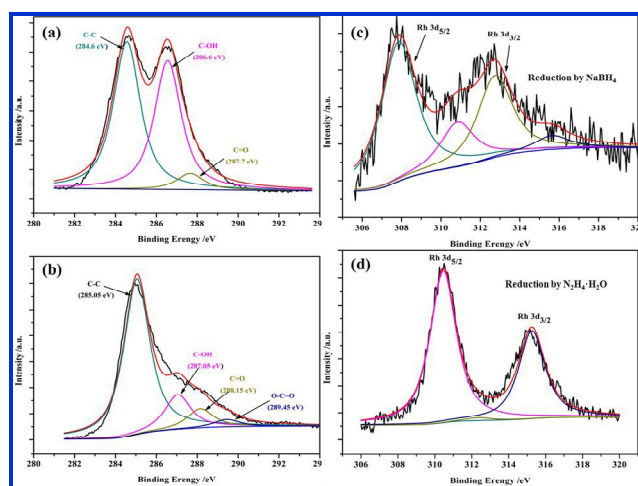


Figure 3 XPS spectra of the C 1s for (a) GO and (b) Rh/RGO; (c, d) Rh 3d for Rh/RGO reduced by different reductant.

The activities of different catalysts for hydrogenation of NBR in a chlorobenzene solution under the same conditions are shown in Table 1. In order to find out whether the RGO carrier was the active center in NBR hydrogenation, the reaction over the RGO carrier was carried out. No degree of hydrogenation (HD) was detected in the absence of Rh NPs, suggesting that Rh was the only active center for NBR hydrogenation.

Compared with other supported catalysts, Rh/RGO revealed excellent activity for hydrogenation of NBR (Table 2, Entry 4). The active Rh NPs well-deposited on the external surface of RGO, which could effectively eliminate the pore diffusion of NBR chain to Rh NPs. The large external surface area of RGO allowed more NBR coils to physically adsorb on its surface, more C=C can be activated. Therefore, the well-deposited Rh NPs and high external surface area of RGO could be the reason for the high activity of Rh/RGO for hydrogenation.

Table 1 The hydrogenation of NBR with various catalyst

Entry	Catalyst	t/h	HD /%
1	Rh/AC	8	28.43
2	Rh/ CaCO ₃	8	32.16
3	Rh/CNT	8	72.48
4	Rh/RGO ^a	6	93.64
5	Rh/RGO ^b	8	8.12

^aThe catalyst reduced by NaBH₄; ^bThe catalyst reduced by N₂H₄·H₂O. All the other catalysts underwent reduction by N₂H₄·H₂O. Reaction condition: T = 120 °C; concentration of Rh = 0.035 wt%; PPh₃ = 0.15 g; 300 mL NBR solution containing 9.0 g of NBR.

However, it was noted that the HD decreased to 8.12% over Rh/RGO reduced with NaBH₄. The different in the activity of the Rh/RGO with different reductant could be attributed to the nature of active species.²⁸ In NaBH₄ system, 79% of Rh NPs are present as Rh⁰ (Table S2), which has low activity towards NBR. For N₂H₄·H₂O system, the most Rh³⁺ in situ reduced to Rh⁺ by PPh₃, which is a highly active specie for hydrogenation of NBR.

In the following investigations, the catalytic system of Rh/RGO reduced with N₂H₄·H₂O and PPh₃ as ligand was used for hydrogenation of NBR. After hydrogenation, the RGO remained in the product of HNBR to form RGO/HNBR composite. The compound formulation and the vulcanizing additives (zinc oxide, stearic acid, sulfur, accelerator M, accelerator TMTD, antiager D and antiager 4010) are listed in Table S3, expressed as parts per hundred parts of rubber (PHR). The tested samples were tailored into dumbbell-shaped in size of 25×3×2 mm³ (Figure S6).

The main mechanical properties of NBR, HNBR and RGO/HNBR with different amounts of RGO are summarized in Table 2. The tensile stress of HNBR is 18.57 MPa, far more than the NBR of 2.37 MPa, which can be attributed to the existence of crystallinity in HNBR.¹ All the tensile stress and tear strength were enhanced for the HNBR/RGO composites. For instance, the HNBR/RGO composites with RGO content range from 0.156 wt% to 1.112 wt% showed a rise in tensile strength up from 8.83% to 44.32%, at maximum stress level of 26.80 MPa more than 18.57 MPa of the parent rubber of HNBR. The improvement in the mechanical properties can be credited to better filler dispersion and good filler-rubber interaction. TEM images in Figure S7 illustrate the state of dispersion of RGO in the HNBR matrix. It can be seen that there is no graphene sheet layer structure in the image of bare NBR or HNBR and the deep black spots are additive. With the increase of RGO content, more and more thin layer remained in RGO/HNBR (the light grey shading represents the continuous RGO). In the Figure S7c~f, it can be seen that RGO sheets are homogeneously inserted into the HNBR matrix. Therefore, a good interfacial interaction between the RGO sheets and the HNBR is very crucial for the nanocomposite to withstand

load.²⁹ Under load, the distributed load by the HNBR matrix is carried predominantly by the RGO fillers.

Herein, it is necessary to compare our results with other reports concerning the graphene-based rubber composites, as listed in Table S4. It is clearly demonstrated that the highly reinforcing efficiency is achieved in our present work. With the addition of only 1.112 wt% of rGO, the tensile strength of the RGO/HNBR composite is up to 26.80 MPa, a increased enhancement of 44% compared with that of unfilled HNBR. A 51 wt% increase in the tensile strength of HXNBR with the addition of 0.44 wt% of GO.³⁰ Zhan incorporated 2 wt% of rGO into NR by solution mixing, and the tensile strength of the rGO/NR composite is improved to 25.2 MPa, while the NR is 17.1 MPa.³¹ Zheng et al. reported a two-fold increase in the tensile strength of NR (14.7 MPa) with incorporation of up to 0.3 wt% of modified GO.³²

Table 3 Electrical volume resistance and volume resistivity of NBR, HNBR and RGO/HNBR composites

Materials	RGO content (wt%)	Volume resistance (×10 ⁷ Ω)	Volume resistivity (×10 ¹⁰ Ω·cm)
NBR	0	10.21	10.42
HNBR	0	11.25	11.43
RGO/HNBR	0.156	9.66	9.85
RGO/HNBR	0.312	7.34	7.45
RGO/HNBR	0.624	5.36	5.34
RGO/HNBR	1.112	4.28	4.17

Table 3 shows the effect of RGO content on electrical volume resistance and volume resistivity of HNBR/RGO composites. Decreased values of volume resistance and volume resistivity were obtained for all the HNBR/RGO composites. The electrical properties of nanocomposites depend primarily on the way the filler particles are distributed through the polymer matrix to form the electrical network. The current studies confirmed the HNBR/RGO composites with RGO content of 1.112 wt% can be used as semi-conductive materials (volume resistivity, 10⁷~10¹⁰ Ω·cm) with volume resistivity of 4.17×10¹⁰ Ω·cm. The lower conductivity is likely due to the defect of the chemical reduction of GO. In previous studies, the material produced from GO is not particularly useful in view of conductor.³³ A completely reduction of GO might be necessary to restore conductivity.

Even though the measured volume resistivity of the HNBR/RGO composites was very low, the composites can offer capacitive field grading from their increased dielectric constant. Figure 4 depicts the variation of dielectric constant (ε') with frequency. The filler of RGO can significantly improve the value of dielectric constant at lower frequency compared with parent rubber of HNBR. But this tendency decreased gradually at higher frequencies. From the Figure S8, it can be seen that the dielectric constant at 10³ Hz is increased from 15.3 for HNBR to 21.7 for composite with 0.624 wt% RGO, and it obviously increases to 37.7 for the composite with 1.112 wt% RGO. And, the dielectric loss of

Table 2 Mechanical properties of NBR, HNBR and HNBR/RGO composites

Materials	HD (%)	RGO content (wt%)	Stress at 100% (MPa)	Stress at 300% (MPa)	Tensile stress (MPa)	Elongation at break (%)	Tear strength (kN/m)
NBR	-	0	0.96±0.1	1.51±0.1	2.37±0.1	450.91±10	9.93
HNBR	96.23	0	0.96±0.1	1.26±0.1	18.57±0.2	610.90±20	10.21
HNBR/RGO	96.18	0.156	0.99±0.1	1.29±0.1	20.21±0.2	628.56±20	11.96
HNBR/RGO	96.54	0.312	0.96±0.2	1.25±0.2	22.14±0.2	685.34±30	12.34
HNBR/RGO	96.68	0.624	1.04±0.2	1.27±0.2	23.12±0.3	720.71±20	13.97
HNBR/RGO	95.97	1.112	1.06±0.2	1.26±0.1	26.80±0.4	850.62±30	15.92

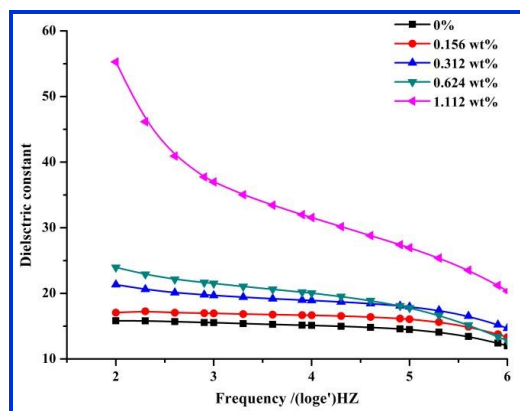


Figure 4 Dielectric constant of HNBR/RGO composites at different RGO contents.

the composite with 1.112 wt% of RGO at 10^3 Hz remains low (0.45).

In summary, for the first time, enhanced mechanical and electrical RGO/HNBR composite was prepared by one-step hydrogenation of NBR with graphene-based Rh catalyst. The catalyst Rh/RGO displayed an excellent hydrogenation activity in the hydrogenation of NBR with low weight content. The as-prepared HNBR/RGO composite exhibits better mechanical and conductive properties compared with that of HNBR. The good mechanical performance of HNBR/RGO composite can be attributed to the good RGO dispersion and RGO-rubber interaction. While, the low conductivity of composites is likely due to the defect of RGO. This approach may be extended for other diene-polymers to prepare the filler-based polymers composites.

Acknowledgements

The financial support of the National Natural Science Foundation of China under Grant No.20774009 is gratefully acknowledged.

Notes and references

^bState Key Laboratory of Organic-Inorganic Composites, Beijing University of Chemical Technology, Beijing 100029, China. Fax: +86-010-64436201; Tel: +86-010-64436201; E-mail: yuedm@nail.buct.edu.cn.

^aKey Laboratory of Beijing City on Preparation and Processing of Novel Polymer Materials, Beijing 100029,

China. Fax: +86-010-64436201; Tel: +86-010-64436201; E-mail: caopbuct2010@163.com

† Electronic Supplementary Information (ESI) available: Experimental section; FTIR spectra; Raman spectra, AFM, SEM and EDS of GO and RGO/Rh; the image of test sample; the vulcanization recipe; TEM of NBR, HNBR and RGO/HNBR; dielectric constant and dielectric loss of RGO/HNBR; XPS data of graphite, GO and Rh/RGO; mechanical properties of graphene-base rubber nanocomposites. See DOI: 10.1039/b000000x/

- H. Wang, L. Yang and G. L. Rempel, *Polymer Reviews*, 2013, **53**, 192-239.
- Y. Kubo and K. Ohura, *US Patent*, 4337329, 1982.
- Y. Kubo and K. Oura, *US Patent*, 4452951, 1984.
- J. S. Parent, N. T. McManus and G. L. Rempel, *Industrial & Engineering Chemistry Research*, 1996, **35**, 4417-4423.
- P. Martin, N. McManus and G. Rempel, *Journal of Molecular Catalysis A: Chemical*, 1997, **126**, 115-131.
- Q. Pan and G. L. Rempel, *Industrial & Engineering Chemistry Research*, 2000, **39**, 277-284.
- K.Y. Han, H.R. Zuo, Z.W. Zhu, G.P. Cao, C. Lu and Y.H. Wang, *Industrial & Engineering Chemistry Research*, 2013, **52**, 17750-17759.
- L. B. Dong, S. Turgman-Cohen, G. W. Roberts and D. J. Kiserow, *Industrial & Engineering Chemistry Research*, 2010, **49**, 11280-11286.
- J. S. Ness, J. C. Brodil, F. S. Bates, S. F. Hahn, D. A. Hucul and M. A. Hillmyer, *Macromolecules*, 2001, **35**, 602-609.
- K. Han, C. Meng, Z. Zhu and G. Cao, *Trans. Tianjin Univ.*, 2014, **20**, 282-291.
- D. Xu, R. G. Carbonell, G. W. Roberts and D. J. Kiserow, *The Journal of Supercritical Fluids*, 2005, **34**, 1-9.
- D. A. Hucul and S. F. Hahn, *Advanced Materials*, 2000, **12**, 1855-1858.
- D. Chen, G.-S. Wang, S. He, J. Liu, L. Guo and M.-S. Cao, *Journal of Materials Chemistry A*, 2013, **1**, 5996-6003.
- X.J. Zhang, G.S. Wang, W.Q. Cao, Y.Z. Wei, J.F. Liang, L. Guo and M.-S. Cao, *ACS Applied Materials & Interfaces*, 2014, **6**, 7471-7478.

15. A. K. Geim, *Science*, 2009, **324**, 1530-1534.
16. C. Lee, X. Wei, J. W. Kysar and J. Hone, *Science*, 2008, **321**, 385-388.
17. S. Moussa, A. R. Siamaki, B. F. Gupton and M. S. El-Shall, *ACS Catalysis*, 2012, **2**, 145-154.
18. K. S. Novoselov, A. K. Geim, S. V. Morozov, D. Jiang, Y. Zhang, S. V. Dubonos, I. V. Grigorieva and A. A. Firsov, *Science*, 2004, **306**, 666-669.
19. Y. Wang, R. Yang, Z. Shi, L. Zhang, D. Shi, E. Wang and G. Zhang, *ACS Nano*, 2011, **5**, 3645-3650.
20. J. Wu, W. Pisula and K. Müllen, *Chemical Reviews*, 2007, **107**, 718-747.
21. A. R. Siamaki, A. E. R. S. Khder, V. Abdelsayed, M. S. El-Shall and B. F. Gupton, *Journal of Catalysis*, 2011, **279**, 1-11.
22. Y. Gao, D. Ma, C. Wang, J. Guan and X. Bao, *Chemical Communications*, 2011, **47**, 2432-2434.
23. B. F. Machado and P. Serp, *Catalysis Science & Technology*, 2012, **2**, 54-75.
24. S. Stankovich, R. D. Piner, X. Chen, N. Wu, S. T. Nguyen and R. S. Ruoff, *Journal of Materials Chemistry*, 2006, **16**, 155-158.
25. H. M. A. Hassan, V. Abdelsayed, A. E. R. S. Khder, K. M. AbouZeid, J. Turner, M. S. El-Shall, S. I. Al-Resayes and A. A. El-Azhary, *Journal of Materials Chemistry*, 2009, **19**, 3832-3837.
26. W. Gao, L. B. Alemany, L. Ci and P. M. Ajayan, *Nature chemistry*, 2009, **1**, 403-408.
27. J. Ohyama, A. Yamamoto, K. Teramura, T. Shishido and T. Tanaka, *ACS Catalysis*, 2011, **1**, 187-192.
28. P. Cao, Y. Ni, R. Zou, L. Zhang and D. Yue, *RSC Advances*, 2015, **5**, 3417-3424.
29. M. Gudarzi and F. Sharif, *CAS Article*, 2012.
30. X. Bai, C. Wan, Y. Zhang and Y. Zhai, *Carbon*, 2011, **49**, 1608-1613.
31. Y. Zhan, J. Wu, H. Xia, N. Yan, G. Fei and G. Yuan, *Macromolecular Materials and Engineering*, 2011, **296**, 590-602.
32. J. Wu, G. Huang, H. Li, S. Wu, Y. Liu and J. Zheng, *Polymer*, 2013, **54**, 1930-1937.
33. H. Kim, A. A. Abdala and C. W. Macosko, *Macromolecules*, 2010, **43**, 6515-6530.